Electronic Supplementary Material (ESI) for Inorganic Chemistry Frontiers.

Supplementary Information

"Double Guarantee Mechanism" of Ca^{2+}-intercalation and rGO-integration Ensures Hydrated Vanadium Oxide with a High Performance for Aqueous Zinc-ion Batteries

Tao Hu[1], Ziyi Feng[1], Yifu Zhang[1,2]*, Yanyan Liu[1], Jingjing Sun[1], Jiqi Zheng[1], Hanmei Jiang[1], Peng Wang[1], Xueying Dong[1], Changgong Meng[1]

[1]*Department of Chemistry, School of Chemical Engineering, Dalian University of Technology, Dalian, 116024, China*

[2]*State Key Laboratory of Fine Chemicals, Dalian University of Technology, Dalian, 116024, China*

*Corresponding author. E-mail address: yfzhang@dlut.edu.cn (Y. Zhang)

Experimental section

Synthesis of graphite oxide (GO)

Graphite oxide (GO) was prepared from natural graphite flakes by an improved Hummer's method [1]. Briefly, 2 g of graphite flakes and 1 g of $NaNO_3$ were dispersed into 46 mL of H_2SO_4 (98 wt.%) under continuous vigorous stirring in an ice bath at about 5 °C. Next, 6 g of fully grinded $KMnO_4$ was added slowly in portions into the mixture whose temperature was controlled below 20 °C and the whole process lasted about 0.5 h. After vigorously stirring for 1 h, remove the ice bath and heat the mixture in a water bath at 35 °C for another 1 h, after which a brown thick solution was obtained. To this, 92 mL of deionized water was added dropwise. Afterwards, raise the temperature to 95 °C and keep it stirred for 15 min, followed by adding 300 mL deionized water and 10 mL H_2O_2 (30 wt.%) to end the reaction, thus a thick golden yellow suspension was obtained. Finally, the GO suspension was diluted and washed with deionized water and 10 wt.% HCl aqueous solution, then repeat with water until pH = 7. Put the dark brown solution to ultrasonic for 1 h and preserve the final product in deionized water. Adjust the volume of water and the GO solution can be obtained.

Materials preparation

All the chemicals with analytically pure were used directly without any further purification. The synthetic process of $Ca_xV_2O_5{\cdot}nH_2O$/rGO (denoted as CaVOH/rGO) is shown in Figure 1a. Firstly, 2 mmol V_2O_5 powder was dissolved in 66 mL deionized water at room temperature under vigorous magnetic stirring. And then 2 mL of H_2O_2 (30 wt.%) was added into the solution slowly. After obtaining a clear orange-red solution, 0.75 mmol $CaCl_2$ powder and 14 mL 20% GO [2] were added into the mixture. The obtained brownish black suspension was further treated by vigorous stir and ultrasonic for 20 minutes, respectively, which were repeated for four times. Then the mixed solution was sealed in a 100 mL Teflon-lined stainless steel autoclave and further maintained at 120 ℃ for 6 h. After cooling to room temperature, the dark green precipitates were collected by suction filtration and washed with deionized water for three times. Finally, the precipitates were freeze dried for 48 hours, and the product CaVOH/rGO was obtained. To compare, the products of $V_2O_5{\cdot}nH_2O$ (denoted as VOH) was also synthesized in the same steps and processes in the absence of Ca^{2+} source.

Characterizations

X-ray diffraction (XRD) patterns were measured using Panalytical X' Pert powder diffractometer at 40 kV and 40 mA with Ni-filtered Cu Kα radiation. The morphology and size of the as-prepared samples were displayed by field emission scanning electron microscopy (FE-SEM, NOVA NanoSEM 450, FEI) and transmission electron microscopy (TEM, FEITecnai F30, FEI). The as-prepared samples were gold-sputtered in advance before TEM observation, and pretreated with ultrasonication so that it could be dispersed in anhydrous ethanol before TEM observation. Energy-dispersive X-ray spectrometer (EDS) and elemental mapping were obtained by a scanning electron microscope (SEM, QUANTA450). X-ray photoelectron spectra (XPS) was collected through an ESCALAB 250Xi electron spectrometer with an excitation source of Al Kα X-ray radiation and the pass energy is 20 eV. The functional groups' stretching and bending information of the samples was characterized by Fouriertransform infrared spectroscopy (FTIR) and recorded on a Nicolet 6700 spectrometer from 4000 to 400 cm^{-1} with a resolution of 4 cm^{-1}. Thermo Scientific spectrometer was used to obtain the chemical bond information by Raman spectrum, with a 532 nm-excitation line. Thermogravimetry analysis (TGA) was conducted on a MTC1000 thermal analysis system from 50 to 1200 ℃ with a heating rate of 5 ℃·min^{-1} under an air atmosphere. The content of element was determined by using inductively coupled plasma-atomic emission spectroscopy (ICP-AES, Optima2000DV, Perkinelmer).

Electrochemical measurements

The electrochemical properties were carried out via stainless steel CR2032 coin-type cells. For the electrode preparation, the cathode electrodes were fabricated by mixing 70 wt.% of active material, 20 wt.% of acetylene black, and 10 wt.% of polyvinylidene fluoride (PVDF) binder in N-methyl-2-pyrrolidone (NMP) and coating the slurry onto titanium foil. And then they were dried under vacuum at 60 ℃ for 9 h. The coin-type cells were assembled by the above cathodes, Zn metal as the anode, 80 μL of 3 M zinc trifluoromethanesulfonate ($Zn(CF_3SO_3)_2$, 98%) aqueous solution as the electrolyte, and a glass fiber filter was used as the separator. The electrochemical performances of the Zn//CaVOH/rGO cells were measured in the voltage range of 0.2-1.5 V (vs. Zn^{2+}/Zn). The cyclic voltammetry (CV) and electrochemical impedance spectroscopy (EIS) were conducted using the CHI-660D electrochemical working station. The galvanostatic and intermittent titration technique (GITT) and the galvanostatic charge-discharge (GCD) test were taken in a multichannel battery testing system (LAND CT201A) to

analyze the reaction and diffusion kinetics and capacity properties, respectively. All the electrochemical characterizations were carried out at room temperature.

Fig. S1

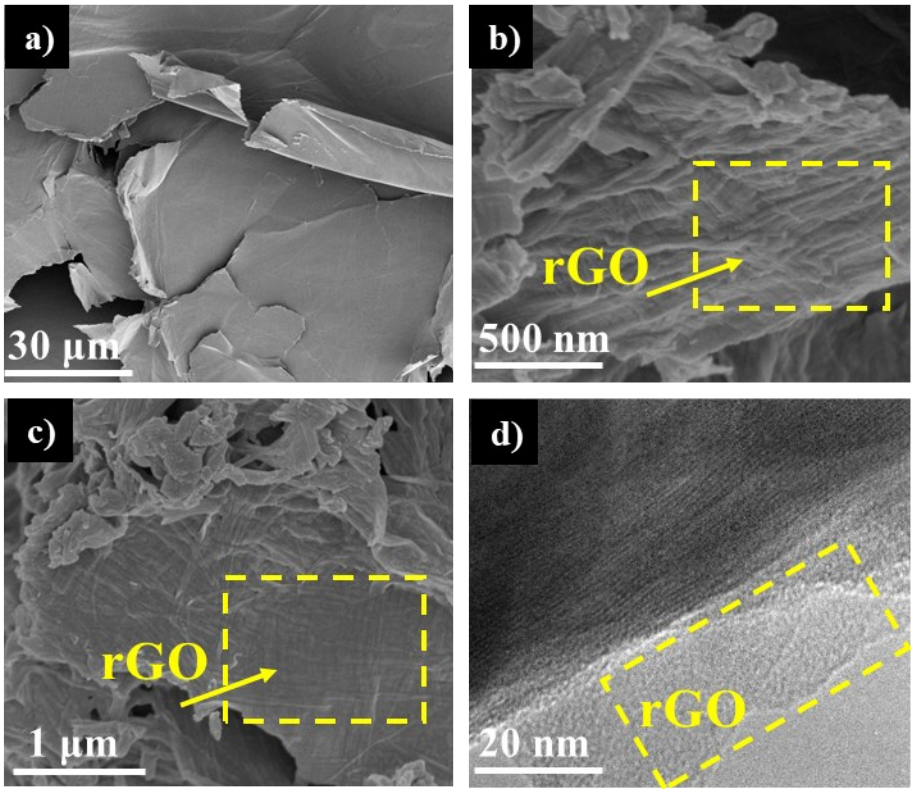

Fig. S1. SEM images of (a) VOH (b)VOH/rGO and (c) CaVOH/rGO; (d) TEM images of CaVOH/rGO

Fig. S2

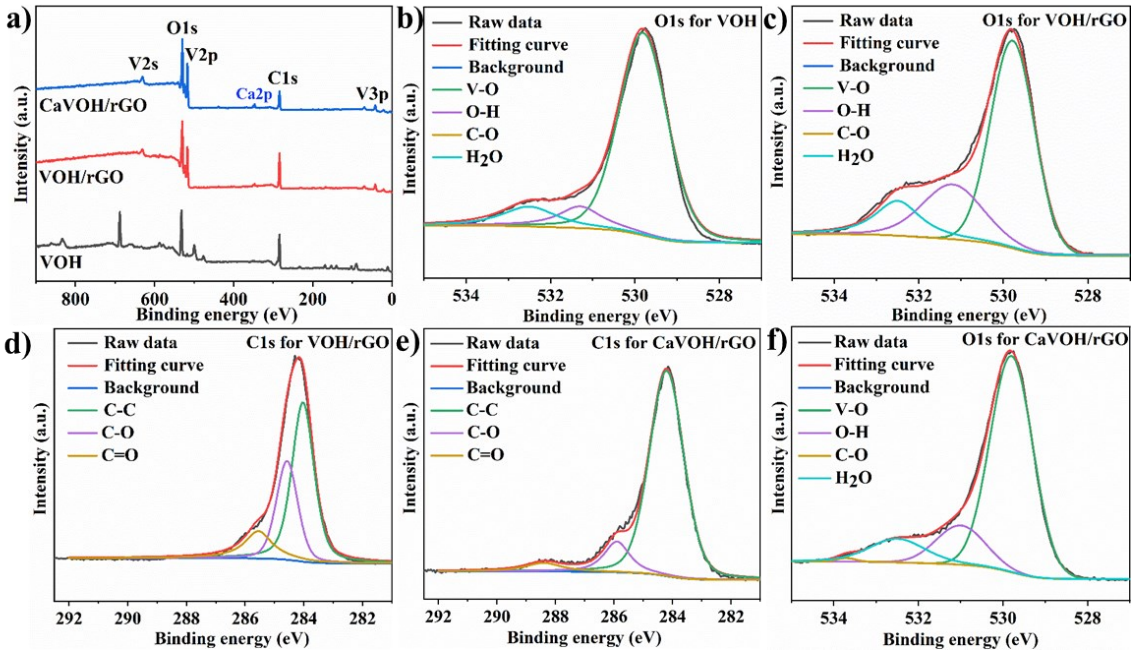

Fig. S2. (a) XPS spectra of VOH,VOH/rGO and CaVOH/rGO; High resolution XPS spectras of (b) VOH, (c-d) VOH/rGO and (e-f) CaVOH/rGO

Table S1

Table S1. Atomic content of Ca, V, O and C in CaVOH/rGO by XPS analysis.

Element	Atomic%
Ca	**1.73**
V	**13.75**
O	**44.71**
C	**39.81**

Table S2

Table S2. Atomic ratio of Ca and V in CaVOH/rGO by ICP analysis.

Element	**ratio**
Ca:V	**0.11:1**

Table S3

Table S3. Weight content of C and H in CaVOH/rGO by EA.

C%	H%	C/H
5.21	2.066	2.5202

Fig. S3

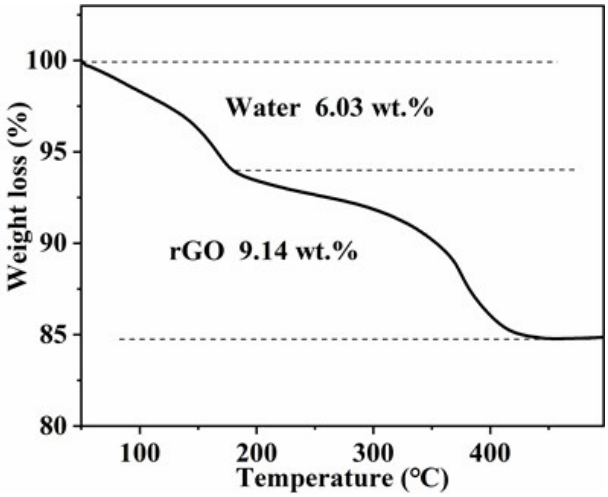

Fig.S3. TGA result of CaVOH/rGO composite.

Fig. S4

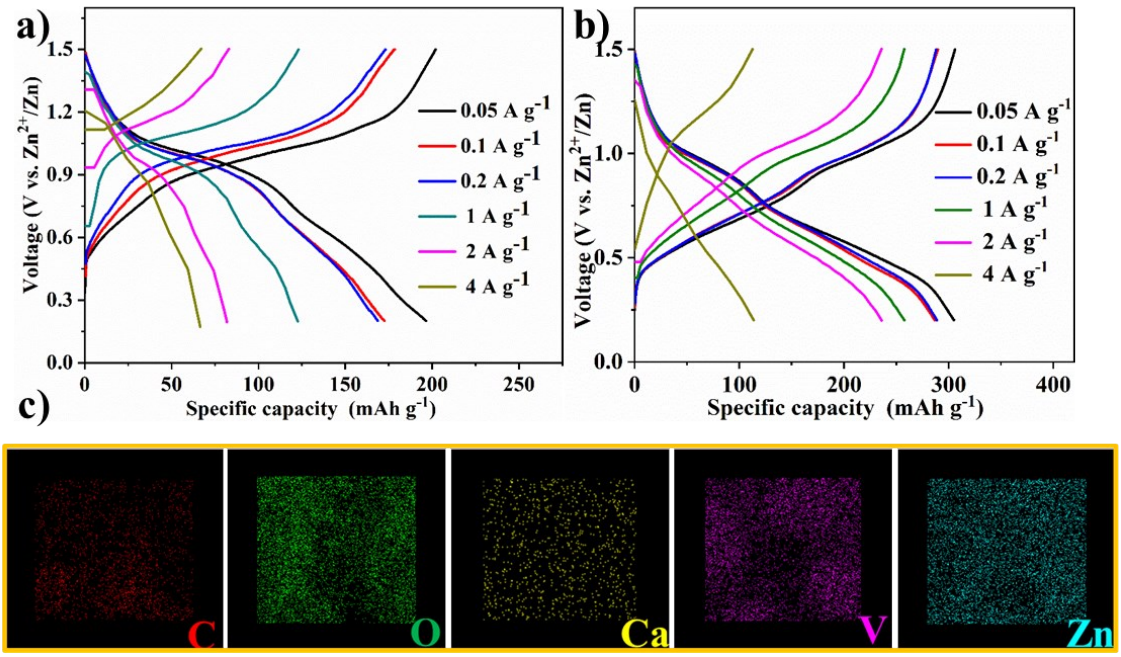

Fig. S4. GCD curves of (a) VOH and (b) VOH/rGO at various current densities. (c) EDS mapping of CaVOH/rGO after 2000 cycles

Table S4

Table S4. Comparison of the specific capacities between the previously reported cathode materials for ARZIBs and this work.

Cathode Materials	Electrochemical Performance	Ref.
CaVOH/rGO	**408, 380, 378, 337, 270 and 269 mA h g^{-1} at 0.05, 0.1, 0.2, 1.0, 2.0, and 4.0 A g^{-1}**	**This work**
$Ba_{1.2}V_6O_{16}\cdot 3H_2O$	321.2,277.3, 247.4, 222.8, 198.2,168.1, 150.7, 129.8, and 108.8 mA h g^{-1} at 0.1, 0.2, 0.3, 0.5, 1, 2, 3, 5, and 10 A g^{-1}	3
$FeVO_4\cdot nH_2O$@rGO	100 mA h g^{-1} at 1.0 A g^{-1}	4
$Cu_3(OH)_2V_2O_7\cdot 2H_2O$	216, 159, 148, 133, 127, and 105 mA h g^{-1} at 0.1, 0.3, 0.5, 0.8, 1.0, and 2.0 A g^{-1}	5
$K_{0.25}V_2O_5$	205,163 and 91 mA h g^{-1} at 1,2,5 A g^{-1}	6
$Mg_{0.34}V_2O_5\cdot nH_2O$	353, 330, 291, 264 and 81 mA h g^{-1} at 0.05, 0.1, 0.5, 1 and 5 A g^{-1}, respectively	7
$Ca_{0.25}V_2O_5\cdot nH_2O$	340, and 289 mAh g^{-1} at 0.2 C and 1C, respectively. (1C=250 mA g^{-1})	8
LiV_3O_8	256, 311, 172, 148, and 47 mAh g^{-1} at 0.016, 0.066, 0.133, 0.266 and 1.066 A g^{-1}, respectively.	9
$Na_{1.1}V_3O_{7.9}$ nanoribbons/graphene	191 mAh g^{-1} at 0.05 A g^{-1}	10
$Na_{0.33}V_2O_5$ nanowire	367.1, 253.7, 173.4, 137.5 and 96.4 mAh g^{-1} at 0.1, 0.2, 0.5, 1, and 2 A g^{-1}, respectively.	11
$Na_5V_{12}O_{32}$ ($Na_{1.25}V_3O_8$)	281 mAh g^{-1} at 0.5 A g^{-1}	12
$HNaV_6O_{16}\cdot 4H_2O$ ($H_{0.5}Na_{0.5}V_3O_8\cdot 2H_2O$)	304 mAh g^{-1} at 0.5 A g^{-1}	12
$Na_2V_6O_{16}\cdot 1.63H_2O$ nanowire	352, 261, and 219 mAh g^{-1} at 0.05, 0.5 and 1 A g^{-1}, respectively	13
$Zn_3V_2O_7(OH)_2\cdot 2H_2O$	200, 122, 84 and 54 mAh g^{-1} at 0.05, 0.5, 1 and 3 A g^{-1}, respectively	14
$Zn_2(OH)VO_4$	204, 160 and 101 mAh g^{-1} at 0.5 C, 10 C and 50 C, respectively. (1 C= 200 mA g^{-1})	15
$Fe_5V_{15}O_{39}(OH)_9\cdot 9H_2O$	385 mAh g^{-1} at 0.1A g^{-1}	16
VO_2(B)/rGO	365 mAh g^{-1} at 0.05 A g^{-1}	17
VO_2(B)	338 mAh g^{-1} at 0.05 A g^{-1}	17
VO_2(B) nanobelts	274 mAh g^{-1} at 0.1 A g^{-1}	18
RGO/VO_2 composite	276 mAh g^{-1} at 0.1 A g^{-1}	19
V_2O_5 nanofibers	319 mAh g^{-1} at 0.02 A g^{-1}	20
$V_6O_{13}\cdot nH_2O$	395 mAh g^{-1} at 0.1 A g^{-1}	21

Fig. S5

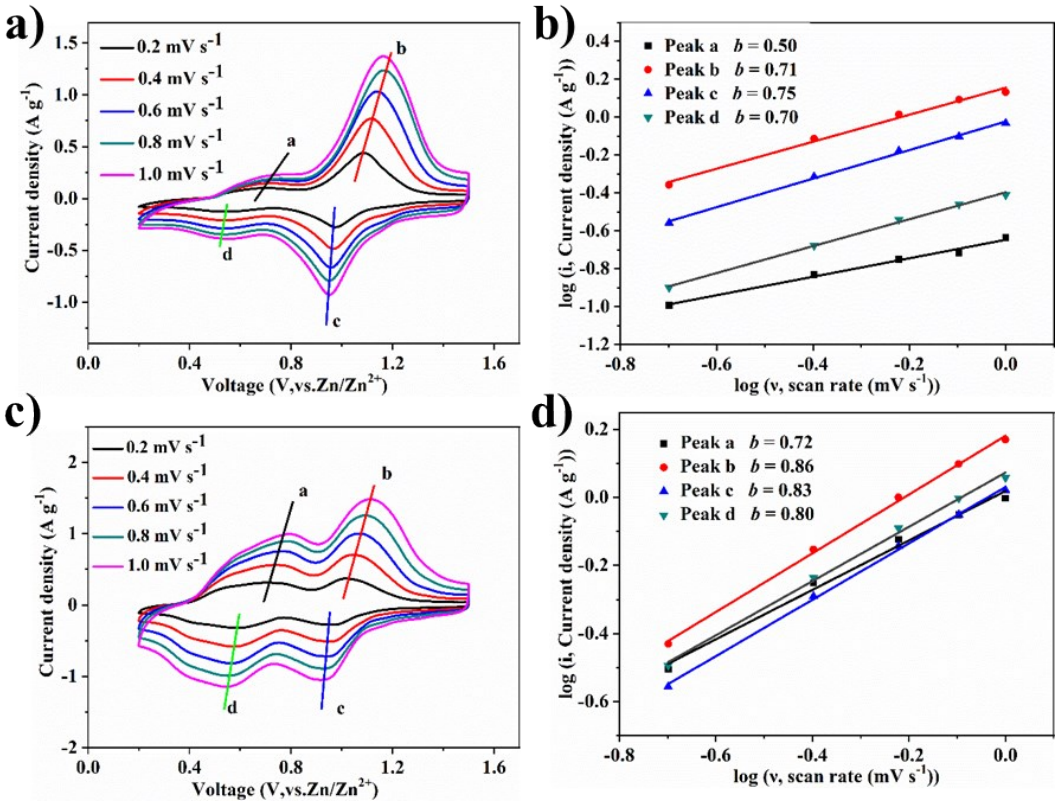

Fig. S5. CV curves at various sweep rates and the relationship between peak currents and sweep rates of (a-b) VOH and (c-d) VOH/rGO.

Fig. S6

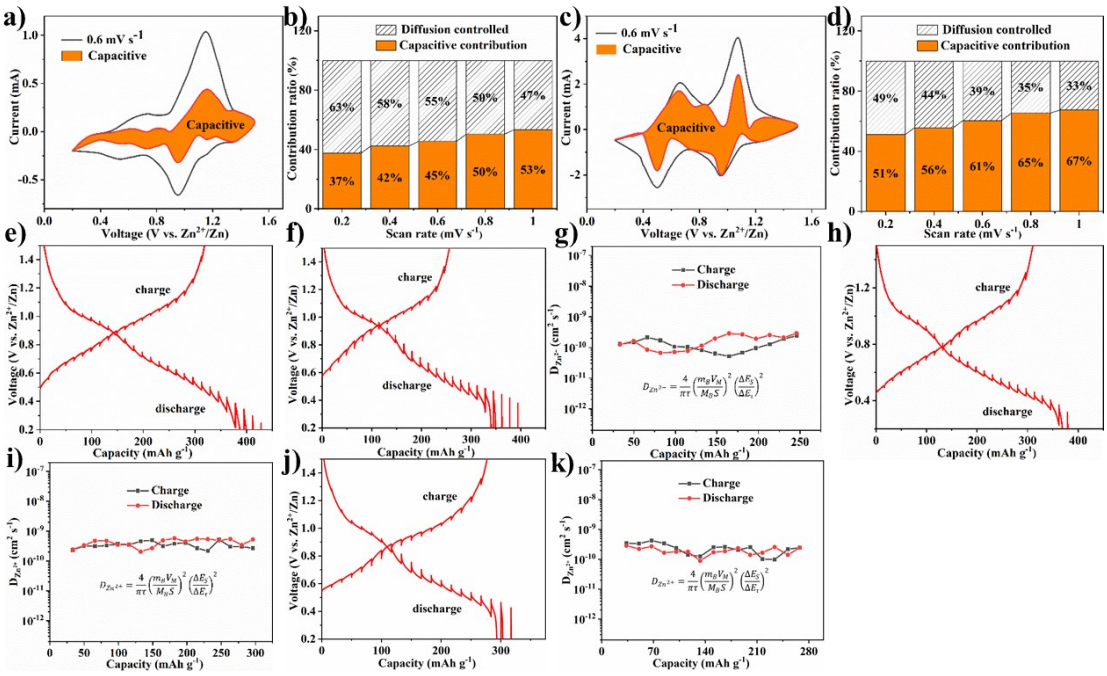

Fig. S6. CV curve of (a) VOH and (c) CaVOH with the calculated capacitive fraction shown by the shaded area at 0.6 mV·s^{-1} and the contribution rate of (b) VOH and (d) CaVOH calculated capacitive at 0.2~1 mV·s^{-1}; the GITT curves of (e) CaVOH/rGO, (f) VOH, (h) VOH/rGO and (j) CaVOH; the corresponding Zn^{2+} (D_{Zn}) diffusion coefficients of (g) VOH, (i) VOH/rGO and (k) CaVOH.

Fig.S7

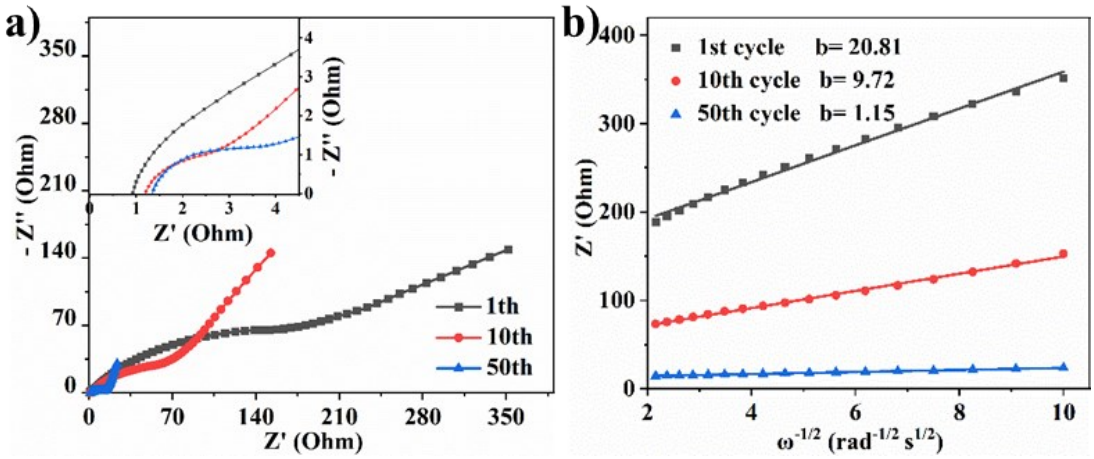

Fig. S7. (a) EIS spectra of CaVOH/rGO; (b) The slopes of the Nyquist plot of CaVOH/rGO battery at low frequencies.

Fig. S8

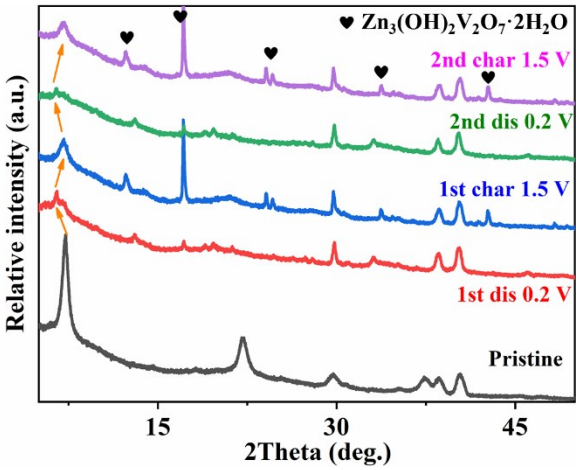

Fig. S8. The *ex-situ* XRD patterns of VOH in the fully discharged and charged states in the first and second cycles

Fig. S9

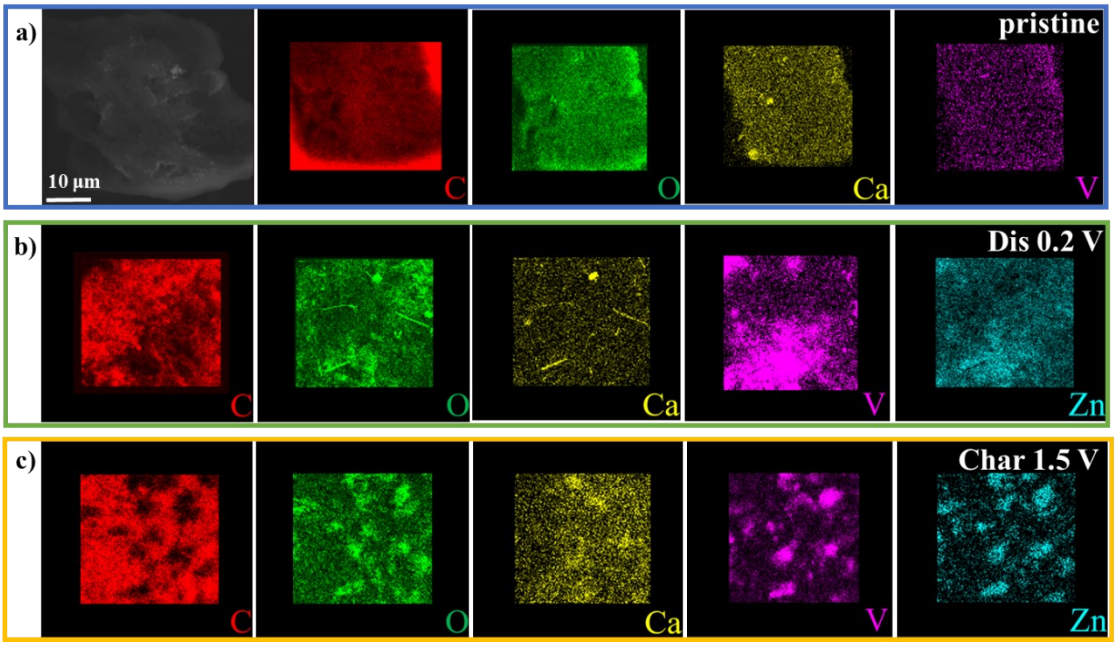

Fig. S9. EDS mapping of CaVOH/rGO in the (a) pristine state, (b) the fully discharged state and (c) the fully charged state.

References

1. W. S. Hummers and R. E. Offeman, Preparation of Graphitic Oxide, *Journal of the American Chemical Society*, 1958, **80**, 1339-1339.
2. T. Hu, Y. Liu, Y. Zhang, M. Chen, J. Zheng, J. Tang and C. Meng, 3D hierarchical porous $V_3O_7{\cdot}H_2O$ nanobelts/CNT/reduced graphene oxide integrated composite with synergistic effect for supercapacitors with high capacitance and long cycling life, *J. Colloid Interface Sci.*, 2018, **531**, 382-393.
3. X. Wang, B. Xi, X. Ma, Z. Feng, Y. Jia, J. Feng, Y. Qian and S. Xiong, Boosting Zinc-Ion Storage Capability by Effectively Suppressing Vanadium Dissolution Based on Robust Layered Barium Vanadate, *Nano Letters*, 2020, **20**, 2899-2906.
4. B. Lan, C. Tang, L. Chen, W. Zhang, W. Tang, C. Zuo, X. Fu, S. Dong, Q. An and P. Luo, $FeVO_4{\cdot}nH_2O$@rGO nanocomposite as high performance cathode materials for aqueous Zn-ion batteries, *Journal of Alloys and Compounds*, 2020, **818**, 153372.
5. L. Chen, Z. Yang, J. Wu, H. Chen and J. Meng, Energy storage performance and mechanism of the novel copper pyrovanadate $Cu_3V_2O_7(OH)_2{\cdot}2H_2O$ cathode for aqueous zinc ion batteries, *Electrochimica Acta*, 2020, **330**, 135347.
6. S. Li, M. Chen, G. Fang, L. Shan, X. Cao, J. Huang, S. Liang and J. Zhou, Synthesis of polycrystalline $K_{0.25}V_2O_5$ nanoparticles as cathode for aqueous zinc-ion battery, *Journal of Alloys and Compounds*, 2019, **801**, 82-89.
7. F. Ming, H. Liang, Y. Lei, S. Kandambeth, M. Eddaoudi and H. N. Alshareef, Layered $Mg_xV_2O_5{\cdot}nH_2O$ as Cathode Material for High-Performance Aqueous Zinc Ion Batteries, *ACS Energy Letters*, 2018, **3**, 2602-2609.
8. C. Xia, J. Guo, P. Li, X. Zhang and H. N. Alshareef, Highly Stable Aqueous Zinc-Ion Storage Using a Layered Calcium Vanadium Oxide Bronze Cathode, *Angewandte Chemie International Edition*, 2018, **57**, 3943-3948.
9. M. H. Alfaruqi, V. Mathew, J. Song, S. Kim, S. Islam, D. T. Pham, J. Jo, S. Kim, J. P. Baboo, Z. Xiu, K.-S. Lee, Y.-K. Sun and J. Kim, Electrochemical Zinc Intercalation in Lithium Vanadium Oxide: A High-Capacity Zinc-Ion Battery Cathode, *Chemistry of Materials*, 2017, **29**, 1684-1694.
10. Y. Cai, F. Liu, Z. Luo, G. Fang, J. Zhou, A. Pan and S. Liang, Pilotaxitic $Na_{1.1}V_3O_{7.9}$ nanoribbons/graphene as high-performance sodium ion battery and aqueous zinc ion battery cathode, *Energy Storage Materials*, 2018, **13**, 168-174.
11. P. He, G. Zhang, X. Liao, M. Yan, X. Xu, Q. An, J. Liu and L. Mai, Sodium Ion Stabilized Vanadium Oxide Nanowire Cathode for High-Performance Zinc-Ion Batteries, *Advanced Energy Materials*, 2018, **8**, 1702463.
12. X. Guo, G. Fang, W. Zhang, J. Zhou, L. Shan, L. Wang, C. Wang, T. Lin, Y. Tang and S. Liang, Mechanistic Insights of Zn^{2+} Storage in Sodium Vanadates, *Advanced Energy Materials*, 2018, **8**, 1801819.
13. P. Hu, T. Zhu, X. Wang, X. Wei, M. Yan, J. Li, W. Luo, W. Yang, W. Zhang, L. Zhou, Z. Zhou and L. Mai, Highly Durable $Na_2V_6O_{16}{\cdot}1.63H_2O$ Nanowire Cathode for Aqueous Zinc-Ion Battery, *Nano Letters*, 2018, **18**, 1758-1763.
14. C. Xia, J. Guo, Y. Lei, H. Liang, C. Zhao and H. Alshareef, Rechargeable Aqueous Zinc-Ion Battery Based on Porous Framework Zinc Pyrovanadate Intercalation Cathode, *Advanced Materials*, 2020, **32**, 1907798.

15. D. Chao, C. Zhu, M. Song, P. Liang, X. Zhang, N. H. Tiep, H. Zhao, J. Wang, R. Wang, H. Zhang and H. J. Fan, A High-Rate and Stable Quasi-Solid-State Zinc-Ion Battery with Novel 2D Layered Zinc Orthovanadate Array, *Advanced Materials*, 2018, **30**, 1803181.
16. Z. Peng, Q. Wei, S. Tan, P. He, W. Luo, Q. An and L. Mai, Novel layered iron vanadate cathode for high-capacity aqueous rechargeable zinc batteries, *Chemical Communications*, 2018, **54**, 4041-4044.
17. J.-S. Park, J. H. Jo, Y. Aniskevich, A. Bakavets, G. Ragoisha, E. Streltsov, J. Kim and S.-T. Myung, Open-Structured Vanadium Dioxide as an Intercalation Host for Zn Ions: Investigation by First-Principles Calculation and Experiments, *Chemistry of Materials*, 2018, **30**, 6777-6787.
18. T. Wei, Q. Li, G. Yang and C. Wang, An electrochemically induced bilayered structure facilitates long-life zinc storage of vanadium dioxide, *Journal of Materials Chemistry A*, 2018, **6**, 8006-8012.
19. X. Dai, F. Wan, L. Zhang, H. Cao and Z. Niu, Freestanding graphene/VO_2 composite films for highly stable aqueous Zn-ion batteries with superior rate performance, *Energy Storage Materials*, 2019, **17**, 143-150.
20. X. Chen, L. Wang, H. Li, F. Cheng and J. Chen, Porous V_2O_5 nanofibers as cathode materials for rechargeable aqueous zinc-ion batteries, *Journal of Energy Chemistry*, 2019, **38**, 20-25.
21. J. Lai, H. Zhu, X. Zhu, H. Koritala and Y. Wang, Interlayer-Expanded $V_6O_{13}\cdot nH_2O$ Architecture Constructed for an Advanced Rechargeable Aqueous Zinc-Ion Battery, *ACS Applied Energy Materials*, 2019, **2**, 1988-1996.